ACCEPTED MANUSCRIPT

Journal of Vacuum Science & Technology B

This is the author's peer reviewed, accepted manuscript. However, the online version of record will be different from this version once it has been copyedited and typeset.
PLEASE CITE THIS ARTICLE AS DOI: 10.1116/6.0005580

3D-Printed polylactic acid (PLA) Mass Spectrometer Deflection Electrode via Copper Electrodeposition

B. Tomasetti,[1] J. Fréreux,[1] T. Corbo,[1] X. Urbain,[1] A. Delcorte,[1] and C. Lauzin[1]
Institute of Condensed Matter and Nanosciences, Université catholique de Louvain, 1348 Louvain-la-Neuve, Belgium

(*Electronic mail: clement.lauzin@uclouvain.be)

(Dated: 19 June 2026)

A 3D-printed polylactic acid (PLA) deflection electrode, featuring an aperture, was copper-coated via electrodeposition following the application of a conductive paint. The electrode was compared to the original stainless steel electrode in a mass spectrometric instrument (STARGATE) across two measurement campaigns separated by three years. Statistical analysis accounting for repeated measurements across ions showed no significant effect of electrode type, campaign year, or their interaction on measured ion intensity. In addition to the temporal stability of the electrode response, deflection of both small and large cluster ions was observed. Pumping curve analysis highlights a slower pumping speed for the copper-coated electrode but shows no significant differences in the final vacuum levels reached in the instrument ($\approx 10^{-8}$ mbar). Furthermore, the aperture-based electrode enables simultaneous use of a Faraday cup and a microchannel plate (MCP) detector, thereby extending the dynamic range of the instrument.

I. INTRODUCTION

In ion optics, instruments often rely on complex electrode geometries, such as hyperbolic electrodes in orbital traps (spindle-shaped central electrode barrel-like outer electrode)[1] or quadrupole ion traps.[2,3] While these designs enhance performance, their fabrication can be a barrier for many laboratories due to limited access to specialized manufacturing tools.

When addressing geometries that are challenging to fabricate using conventional machining techniques, additive manufacturing offers a compelling alternative, owing to the widespread availability and cost-effectiveness of modern 3D printing technologies. In particular, processes such as stereolithography (SLA) can achieve high dimensional accuracy, with feature resolutions reaching the micrometer scale.[4,5]

However, despite this level of precision, the resulting materials are typically electrically insulating. Consequently, additional strategies must be developed to impart electrical conductivity to the fabricated structures.[6]

Among these 3D printing strategies, fused filament fabrication (FFF)[7] with the use of composite filament[8] enabled the production of small conductive electrodes. Alternatively, direct 3D printing of metals for electrode fabrication can be achieved using powder bed fusion techniques such as selective laser melting (SLM).[9] However, these methods are not ideal for fabricating large, smooth electrodes. SLM typically produces rough, grainy surfaces and requires extensive post-processing, in addition to being limited by high investment and operational costs. FFF using composite filaments suffers from poor resolution and challenges in producing homogeneous conductive parts due to the heterogeneous nature of the material (*e.g.*, brittle carbon-filled PLA). Nevertheless, promising ion optic elements have been realized using conductive PLA (Proto-pasta by ProtoPlant), including quadrupole and einzel lenses[10], deflectors[11,12], and ambient-pressure ion mobility spectrometers.[13,14] These structures, however, exhibit high electrical resistance and are therefore unsuitable for carrying high electric currents. Recent advances in material formulation[15] may overcome these limitations; for example, Electrifi filament, with a resistivity as low as 0.006 $\Omega\cdot$cm[16], has been used to 3D print a quadrupole mass filter.[17]

3D printing has revolutionized tool development in mass spectrometry[18], primarily through applications in external[19,20] and internal[21,22] sample handling and automation[23,24], as well as in fabricating 3D-printed mechanical housings for conductive ion optic elements.[3,25] However, its use for direct ion manipulation remains relatively limited due to the challenges described above.

For miniaturized ion optics, high-resolution 3D printing based on two-photon polymerization (2PP), combined with electron-beam evaporation coating, is highly effective.[26] However, in this proof-of-principle study, the manufacturing method is demanding in terms of equipment, as it requires a femtosecond laser, a microscopic objective, and an electron-beam evaporation setup. In 2017, a beam splitter for polar neutral molecules consisting of an electrostatic hexapole guide that smoothly transitions to two bent quadrupoles was fabricated via SLA and subsequent electroplating.[4] The structure was printed in one piece, allowing precision defined by the printer resolution. However, electroplating was carried out using an unknown combination of chemical and electrolytic procedures by a plating company (Galvotec GmbH, Switzerland), which increased production time and cost. For more complex geometries and improved control over coating thickness, SLA printing can be combined with electroless metal plating following preliminary chemical activation of the surface, as described in Refs.[27–29]. In particular, electroless plating prior to electrodeposition has enabled the fabrication of radiofrequency (RF) coils with homogeneous and tunable copper coatings.[29] Such hybrid approaches that combine electrodeposition with chemical activation have also been reported[30–32], although they are more demanding to implement.

In this work, we demonstrate that a standard PLA 3D printer (Flsun V400), combined with a simple electrodeposition method using conductive paint, enables the fabrica-

ACCEPTED MANUSCRIPT
Journal of Vacuum Science & Technology B
This is the author's peer reviewed, accepted manuscript. However, the online version of record will be different from this version once it has been copyedited and typeset.
PLEASE CITE THIS ARTICLE AS DOI: 10.1116/6.0005580

tion and metallization of an apertured deflection electrode for a mass spectrometer (STARGATE) within a single working day. This instrument enables high-resolution photodissociation spectroscopy of cold ionic species, employing a 90° ion deflection coupled to time-of-flight mass spectrometry.[33] The goal is to show that additive manufacturing and coating strategies can be used to rapidly test ion optics designs in high-vacuum instruments, particularly for geometries that are difficult to fabricate using conventional methods.

II. MATERIAL AND METHODS

A. Electrodeposition

Electrodeposition (also called electroplating) of copper is a process in which a copper layer is deposited onto an electrode by passing an electric current through an electrolyte solution containing copper ions (Cu^{2+}). This process follows the principles of electrolysis. The anode (positive electrode) is a copper plate (Cu), which will dissolve and supply Cu^{2+} ions to the solution. The cathode is the object on which copper will be deposited. Copper ions from the solution gain electrons and deposit as solid copper. Both electrodes are placed in an acidic bright copper plating solution (Tifoo, MARAWE GmbH & Co. KG), consisting of a commercial $CuSO_4/H_2SO_4$-based electrolyte containing organic brightening additives and chloride ions. The exact formulation is not publicly disclosed by the manufacturer. However, such baths typically contain copper sulfate as Cu^{2+} ions source, sulfuric acid as supporting electrolyte, and trace chloride ions and organic additives to promote fine-grained, bright deposits. A DC power source is used to drive the electrochemical reaction. A current of around 100 mA flows (0.2 – 1 V) and varies during deposition. Fig. 1(a) shows the deposition set-up. The primary challenge was ensuring sufficient cathode conductivity to facilitate electron flow. This was achieved by applying a conductive colloidal paint (Fig. 1(b), Tifoo) to the PLA surface prior to electrodeposition. The electrode was manually repositioned during the coating process to ensure complete surface coverage. The bath temperature and total deposition time were not recorded (approximately 5 h), which should be monitored and controlled in future experiments to improve reproducibility. Post-coating polishing is also recommended, particularly for high-vacuum applications where surface smoothness is critical. Here, the electrode was first polished with medium sandpaper (P300) and then ultra-fine sandpaper (P1200). Finally, the coating thickness was measured using optical microscopy and found to be approximately 90 µm. The thickness appears relatively homogeneous across the electrode, and optical images are provided in the supplementary material (see Fig.S7).

B. STARGATE and electrode general description

The printed and subsequently coated electrode was installed in the STARGATE instrument shown in Fig. 2. Briefly, STARGATE combines a pulsed supersonic expansion source with a time-of-flight mass spectrometer, pulsed ion deflection, and a nanosecond pulsed dye laser, enabling photodissociation spectroscopy of molecular cations.

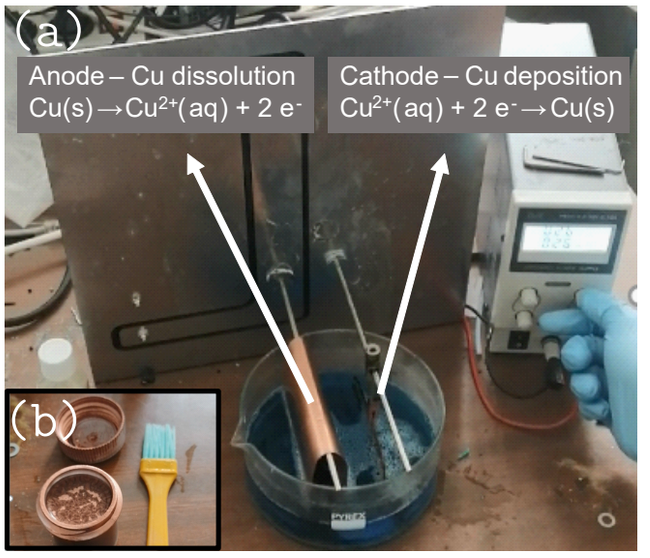


FIG. 1. (a) Picture of the electrodeposition set-up. A DC current is provided to drive the reaction. (b) Copper conductive varnish (Tifoo) used to coat the electrode.

The ion source (1) consists of a pulsed supersonic expansion coupled to an ionization mechanism, either an electric discharge or an electron gun. After passing through a skimmer (2), the ions are accelerated, bunched, and gated by a series of electrodes (3). The ion beam is then focused by an einzel lens (4), after which a two-dimensional deflector (5) can be used for mass selection or beam deflection. A second stage of differential pumping (6) is located upstream of the interaction region, where the ions are irradiated by a pulsed dye laser before entering the energy analyzer.

The energy analyzer consists of two curved electrodes: an internal electrode (8) and an external electrode (9). The external electrode was replaced by the printed and coated electrode developed in this work. Finally, the ions are either detected by a microchannel plate detector stack (11) or allowed to continue along a straight trajectory toward a sample or a secondary detector. A more detailed description of the instrument can be found in Refs.[33,34].

To allow ions to follow an undeviated trajectory, the external electrode requires a 12 mm aperture machined on a curved surface. This presents several compounding difficulties: the aperture axis is nearly tangent to the local surface profile, forcing shallow tool engagement where deflection and chatter degrade both dimensional tolerance and edge quality; the curved geometry provides no flat datum for workholding, increasing the risk of part displacement; and achieving a clean aperture rim — critical to avoid local field distortion — requires a geometrically constrained finishing pass. These challenges are compounded for one-off prototype parts where dedicated fixturing is not economically justified. By contrast, 3D printing produces the aperture and curved body in a single operation

ACCEPTED MANUSCRIPT
Journal of Vacuum Science & Technology B
This is the author's peer reviewed, accepted manuscript. However, the online version of record will be different from this version once it has been copyedited and typeset.
PLEASE CITE THIS ARTICLE AS DOI: 10.1116/6.0005580

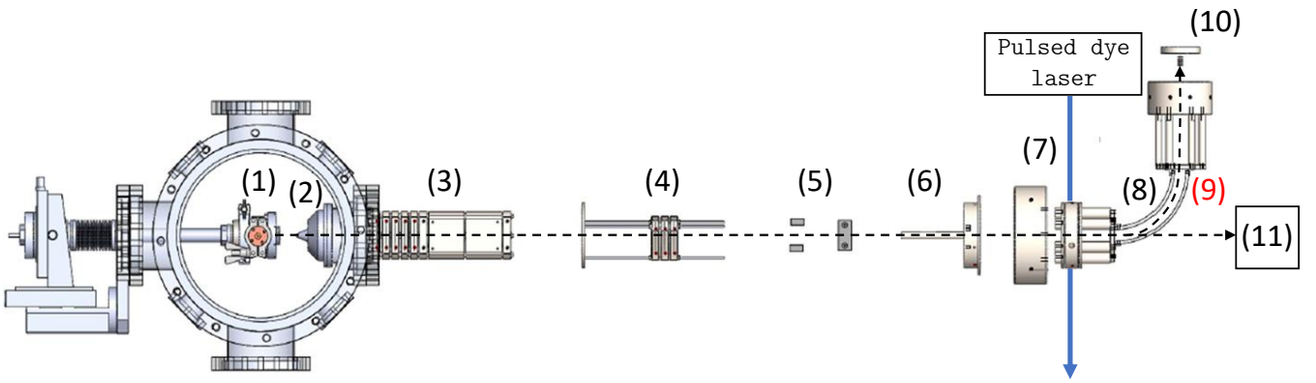


FIG. 2. Design of the STARGATE instrument with (1) the source of ionic compounds, (2) skimmer, (3) electrostatic extraction and lens coupled to an ion gating, bunching, and re-referencing unit, (4) electrostatic lens, (5) pulsed 2D deflector, (6) differential pumping tube, (7) laser and ion beam interaction region, (8) internal electrode and (9) external electrode of the 90° cylindrical energy analyzer, (10) MCP detector and (11) sample holder or second detector. A detailed description of the optical bench with the pulsed dye oscillator pumped by a Nd:YAG laser used for photodissociation spectroscopy can be found in Ref.[33]

with no tool engagement or fixturing constraints, making it inherently better suited to this geometry.

C. Measurements performed with STARGATE instrument

In this work, for the spectra in Fig. 3, CO_2 at 3.2 bar was bubbled through liquid H_2O, and the resulting CO_2/H_2O mixture was introduced into the supersonic expansion. The pressure in the jet chamber was 4.86 x 10^{-5} mbar, the pressure after the skimmer was 6 x 10^{-6} mbar, and the pressure at detection was 8.4 x 10^{-8} mbar during the measurement using the copper-coated electrode. The pulsed valve was set at 30 Hz with a pulse width of 60 µs and a pulsed voltage of -120 V. An electron gun (3.1 A, 5.52 V) is used to ionize the molecules. The electron gun has a collector (+20 V) and two focusing electrodes (-56 V). The pulses were bunched after 166 µs by switching the first bunching electrodes from -1000 V to +150 V and the second bunching electrode from -1000 V to 0 V. A table with all the timing and voltages of the instrument can be found in the supplementary material (see Table SII). H_2O^+ (19.25 µs), CO_2^+ (29.73 µs), $(CO_2)_2^+$ (42.02 µs) and $(CO_2)_3^+$ (51.25 µs) were used to calibrate the spectra. The multichannel plate (MCP) detector was biased at -1500 V, and the signal was amplified by a factor of 2 after detection.

For Ar expansion (3 bar) in Fig. 5, the pulse width was 120 µs. The electron gun was operated under the same conditions (3.1 A, 5.52 V), with the collector and focusing electrodes biased at +20 V and -60 V, respectively. The pressure in the jet chamber was 5.86 x 10^{-5} mbar, the pressure after the skimmer was 1.88 x 10^{-5} mbar, and the pressure at detection was 5.7 x 10^{-8} mbar. The pulses were bunched after 203 µs by switching the first bunching electrodes from -1000 V to +140 V and the second bunching electrode from -1000 V to 0 V. The extraction voltage was set to -184 V and the Lens 1 to -1000 V. The external 90° deflection electrode was set to +194 V when the ions are deflected toward the MCP and set to 0 V when the deflection was off (the ions reach the Faraday collector). The internal 90° deflection electrode was set to -174 V and switched to 0 V when the deflection is off. H_2O^+ (19.2 µs), Ar^+ (28.45 µs), Ar_2^+ (40 µs), Ar_3^+ (49 µs) were used to calibrate the spectra. The MCP detector was biased at -1558 V.

III. RESULTS AND DISCUSSION

A. Electrodes comparison

Fig. 3 shows the mass spectra obtained for (a) the stainless steel electrode and (b) the copper-coated electrode. Fig. 3(c) shows a picture of both electrode with the stainless steel one above.

For both spectrum, a CO_2/H_2O expansion at 3.2 bar was used to create cations accelerated at -1 keV toward an MCP detector positioned downstream of the deflection stage. STARGATE parameters (see Table SII in supplementary material) where kept identical for both measurements. A voltage of +194 V was applied to the external deflection electrode producing nearly identical mass spectra, with only minor variations in signal intensity, confirming that both electrode configurations efficiently deflect the ions.

The integrated area was computed by trapezoidal integration of a baseline-corrected signal over a $\pm$ 1 FWHM window around each apex. For CO_2^+, the integrated intensities were 575 (a.u.) for the copper-coated electrode and 637 (a.u.) for the stainless steel (inox) electrode, yielding a Cu/Inox ratio of 0.90. However, for the cluster $(CO_2^+)_3$, the Cu/Inox ratio is equal to 1.08.

This variation in signal intensity may originate from several factors. As the voltage and pressure conditions were the same, these sources of variation should be limited. However, the variability could arise from the change of the electrode, variations in the valve temperature over time (heating due to

ACCEPTED MANUSCRIPT
Journal of Vacuum Science & Technology B
This is the author's peer reviewed, accepted manuscript. However, the online version of record will be different from this version once it has been copyedited and typeset.
PLEASE CITE THIS ARTICLE AS DOI: 10.1116/6.0005580

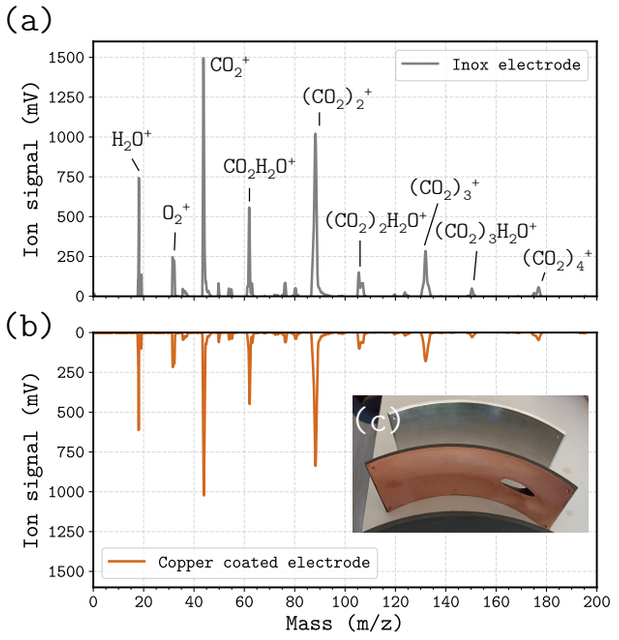


FIG. 3. CO_2/H_2O mass spectra obtained using the (a) stainless steel deflection electrode and (b) the PLA-coated electrode. (c) Photograph of the different external electrodes.

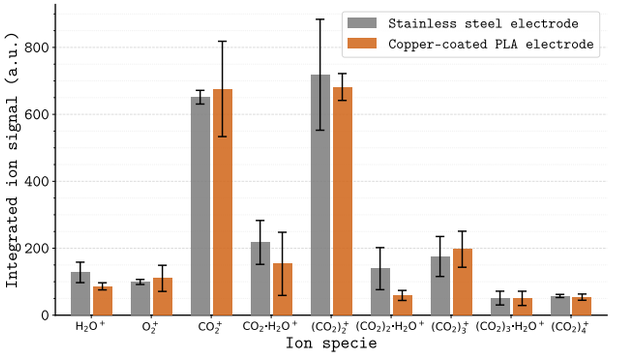


FIG. 4. Integrated ion signal (a.u.) of the CO_2/H_2O mass spectra obtained using the stainless steel deflection electrode (grey) and the PLA-coated electrode (orange). Each intensity is an average over two sets of measurements separated by three years,Each intensity is an average over two sets of measurements separated by three years, and the error bars represent the variation between these two sets. The integrated area was computed by trapezoidal integration of a baseline-corrected signal over a ± 1 FWHM window around each apex.

the electron gun and cooling due to expansion), the amount of water introduced into the mixture, and the distance between the piezo and the nozzle. The latter parameter is adjusted via an external screw, which is manually changed without recording its position.

To evaluate the long-term stability and determine whether the electrode change has an impact on the spectrum, the same comparison was performed three years after its installation. During this period, the electrode remained in the instrument, and a rotationally resolved spectrum of H_2O-Ar was successfully recorded (data not shown). A change in the electrode color toward a more bluish appearance was observed, likely due to the absence of a protective layer deposition and repeated exposure to atmospheric air between pump-down cycles. Fig. 4 shows the integrated ion signal averaged over the two sets of measurements for several identified ion species. It can be seen that the change of electrode does not have a significant impact on the signal intensities. In addition, the stability of the electrode over time was demonstrated. The spectra comparison obtained during the 2026 campaign and a table listing all the instrument parameters are shown in the supplementary material.

A mixed linear model accounting for repeated measurements across ions showed that neither electrode type, campaign year, nor their interaction had a statistically significant effect on intensity. Specifically, no significant differences were observed between stainless steel and copper-coated electrodes ($p = 0.289$), between the 2023 and 2026 campaigns ($p = 0.991$), or in the electrode–time interaction ($p = 0.576$), where p-values above 0.05 indicate that the observed differences are consistent with random variation. Overall, the results suggest that intensity is dominated by ion-specific behavior, while electrode material and temporal variation between campaigns do not have a measurable impact within the current dataset.

It is worth noting that the mass resolving power (FWHM-based), averaged over all identified ion species, decreases from 136.9 to 74.7 for the stainless steel electrode between the 2023 and 2026 campaigns, whereas it decreases from 104.2 to 58.5 for the copper-coated electrode. Both electrodes exhibit a similar relative decline, suggesting that the loss in resolution is likely driven by instrumental or operational factors rather than by the electrode material alone. Indeed, the mass resolving power is highly sensitive to ion bunching conditions, which were not optimized here in order to maintain identical experimental constraints. By adjusting the bunching voltage, higher mass resolving power could likely be achieved in the 2026 campaign. This supports the idea that long-term changes in instrument conditions (*e.g.*, alignment, wear of the source) may have a stronger influence on resolving power than the choice of electrode.

Finally, profilometry measurements were performed on the electrode surfaces. The corresponding profile plots, texture parameters and images are provided in the supplementary material (Fig.S5, Fig.S6 and Table SIII). The copper-coated electrode exhibited a roughness P_a of 5.12 µm, compared to 0.33 µm for the stainless steel electrode. Although this difference is relatively significant, the surface state of the copper-coated electrode was considered sufficient based on the observed spectral quality and vacuum performance. However, alternative polishing strategies, such as lapping films or vibratory finishing, could be employed to achieve smoother surfaces.

ACCEPTED MANUSCRIPT
Journal of Vacuum Science & Technology B
This is the author's peer reviewed, accepted manuscript. However, the online version of record will be different from this version once it has been copyedited and typeset.
PLEASE CITE THIS ARTICLE AS DOI: 10.1116/6.0005580

B. Function and Performance of the Electrode

The following experiment demonstrates the utility of an external apertured electrode. First of all, this type of electrode can be used to compare detectors in pairs, enabling the simultaneous comparison of deflected and direct beam signals. A Faraday collector is positioned in the beam path, and its signal is compared to that of the MCP detector placed after deflection. When a charged particle strikes the collector, it neutralizes by transferring its charge to the metal surface. This charge is then measured as a current via an operational amplifier with a gain of 5 x 10^{12} V/A. The key advantage is the direct proportionality between the measured current and the number of incident ions, enabling precise quantification of ion abundance.

Fig. 5 illustrates the detection setup alongside a mass spectrum obtained using both the Faraday collector and the MCP detector. A slight time-of-flight shift is observed due to the minor difference in detector path lengths.

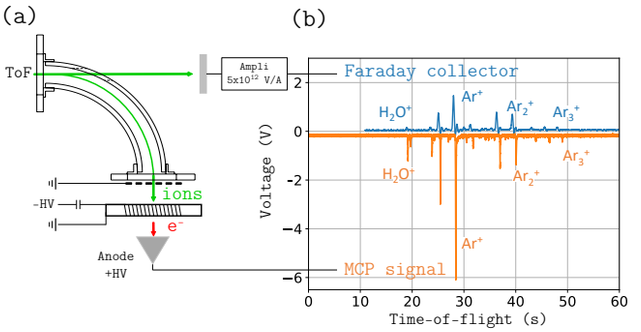


FIG. 5. (a) Schematic illustration of the deflection electrodes, which guide the beam either toward a Faraday collector or a MCP. The perforated deflection electrode was 3D printed and coated with copper. (b) Mass spectra of an identical beam detected using the Faraday collector (blue) and the MCP (orange).

While the Faraday collector performs as expected, it exhibits lower sensitivity and a slower effective response, due to the bandwidth limitations of the current amplifier, compared to the MCP. The combination of the MCP and the Faraday cup provides a significantly broader dynamic range: the main species can be detected using the current amplifier, while trace species are measured with the MCP. The aperture will be particularly useful for photodissociation experiments[33], where energy separation of the products is required. In this case, on-axis transmission through the aperture is well suited for primary ion time-of-flight spectra.

Then, the apertured electrode can be used for large cluster deposition and soft-landing.[35] Indeed, a cluster size distribution can be measured using the MCP detector in combination with beam deflection using STARGATE. When the deflection is turned off, the cluster beam can instead be directed onto a sample placed in the straight beam path. A cluster distribution centered around Ar_{625}^+ (1 keV) was measured with the apertured electrode prior to sample irradiation (see Fig.S4 in the supplementary material). However, at this energy, the efficiency of the MCP decreases significantly for such large ions, and the signal is therefore relatively low. Post-acceleration could extend the detection range of STARGATE, particularly if large clusters are to be detected in future experiments.

C. Vacuum considerations for 3D-printed electrodes

Electrodes fabricated from PLA by 3D printing and coated with copper impose specific constraints for vacuum operation. The polymer substrate exhibits higher outgassing than bulk metals due to trapped gases, residual volatiles, and the intrinsic porosity of FFF structures. While the copper coating provides electrical conductivity and acts as a partial diffusion barrier, it does not completely eliminate outgassing. This limitation can arise from microdefects or discontinuities in the coating, insufficient coating thickness, or partial coverage of the PLA substrate, as is the case in the present work.

Vacuum compatibility, compared to fully metallic electrodes, is therefore still questionable. However, for moderate vacuum levels (*i.e.*, high vacuum, $\sim 10^{-6}$–10^{-8} mbar), it has already been demonstrated that PLA used in 3D printing is vacuum compatible. In Ref.[25], residual gas analysis and pump-down curve measurements were performed on PLA samples. No significant changes in gas composition were observed, and the pump-down curves reached comparable ultimate vacuum levels, with only minor differences in pumping speed. We also performed a residual gas analysis (see Fig.S8 in the supplementary material) and arrived at the same conclusion for the outgassing. Then, pumping curves were recorded for the copper-coated electrode and compared with those obtained for the stainless steel electrode. A difference in pumping time was observed (5 h 15 min to reach 2 x 10^{-7} mbar for the stainless steel electrode, compared to a longer time of 22 h 28 for the copper-coated electrode), although the final vacuum level achieved was equivalent. The pumping curves and a detailed discussion are provided in the supplementary material.

However, reaching ultra-high vacuum (UHV, $< 10^{-8}$ mbar) is unlikely without additional treatments. Bake-out procedures must also be carefully controlled: while mild heating (< 50–$60\,^{\circ}$C) can help reduce surface contamination and desorb water, higher temperatures risk deforming the PLA substrate (glass transition temperature and degrading the metal coating adhesion. Pre-conditioning steps such as prolonged pumping, low-temperature baking, or surface sealing (*e.g.*, thicker metal coating or intermediate barrier layers) can improve performance and were not applied in the present work.

For STARGATE, the electrode is compatible with operation because a sufficient vacuum level of $\sim 10^{-8}$ mbar is achieved in the deflection and detection region, which is separated from the rest of the system by differential pumping (see Fig. 2) and is pumped by a 685 L/s (N_2) HiPace 700 turbomolecular pump located below the electrodes.

ACCEPTED MANUSCRIPT
Journal of Vacuum Science & Technology B
This is the author's peer reviewed, accepted manuscript. However, the online version of record will be different from this version once it has been copyedited and typeset.
PLEASE CITE THIS ARTICLE AS DOI: 10.1116/6.0005580

D. Application scope

This section aims to delineate the scope and applicability of the method developed in the present work. The approach is compatible with any vacuum instrument operating at pressures of 10^{-8} mbar or above, including mass spectrometers, ion guides, deflectors, and related devices. For ultra-high vacuum (UHV) applications, copper-coated PLA electrodes may remain viable provided additional strategies are implemented, such as full surface encapsulation of the polymer, miniaturisation of the electrode geometry, and optimized polishing protocols to minimize outgassing and surface porosity. These avenues were not explored in the present study but represent natural extensions of this work.

A key advantage of the proposed method lies in its cost-effectiveness and rapid prototyping capability. The ability to design, print, and test a functional electrode within hours — rather than waiting days to weeks for conventional machining or external manufacturing — considerably accelerates the experimental development cycle. As a concrete example, an apertured electrode geometry was conceived in this work to investigate the sputtering of biomolecules using large cluster projectiles. In this configuration, a deflection stage is used to characterize the cluster size distribution and acquire mass spectra, while the aperture allows the selected cluster beam to reach the target sample downstream. Obtaining such a custom electrode directly from an in-house 3D printer, without relying on external suppliers or complex manufacturing constraints, represented a significant practical advantage.

Finally, this method holds particular promise for the fabrication of electrodes with complex or mathematically defined geometries. Devices such as Orbitrap analyzers, whose electrode profiles are governed by a specific mathematical function, as well as quadrupole, hexapole, and higher-order multipole ion optics, require precise and often intricate shapes that are traditionally expensive to machine. Additive manufacturing combined with conductive coating offers a compelling route to prototype and validate such geometries at a fraction of the conventional cost, opening new possibilities for custom ion optical designs in academic and small-scale research environments.

IV. CONCLUSION AND FUTURE PROSPECTS

A deflection electrode for the STARGATE instrument was fabricated by 3D printing in PLA, followed by copper electrodeposition. The key advantage of the printed design lies in its beam-aligned aperture, which enables undisturbed ion propagation when deflection is off, thereby unlocking new experimental configurations. Spectral comparisons between the original stainless steel electrode and the copper-coated electrode show no significant differences in intensities, even after a second measurement campaign performed three years after the initial installation of the copper-coated electrode.

The integration of the electrode does not compromise vacuum performance of STARGATE instrument, maintaining high vacuum conditions in the electrode and detection region with pressure in the 10^{-8} mbar range. No outgassing species attributable to PLA were identified in residual gas analysis. However, a reduction in pumping speed was observed when comparing both electrodes.

Current limitations include control over copper layer thickness and homogeneity, which could be improved through solution stirring and automated electrode rotation during deposition. Further improvements may be achieved using more advanced chemical treatments, such as electroless copper plating or an improved graphite-based paint formulation, as detailed in Ref.[36] However, the combination of conductive paint and electrodeposition provides a rapid and low-cost alternative, enabling straightforward metallization of 3D-printed structures without complex chemical processing, while also serving as an effective seed layer for subsequent electrodeposition.

Finally, a single-step electrodeposition process on conductive plastic filaments (*e.g.*, Electrifi, with a resistivity of 0.006 Ω.cm) could further simplify fabrication.[16] Emerging materials with enhanced properties may also expand design possibilities of this proof of concept.

SUPPLEMENTARY MATERIAL

Sec. I provides drawings of the deflection electrodes and photographs of their installation. Sec. II evaluates the temporal stability and repeatability of the electrodes. Sec. III describes the detection of large clusters. Sec. IV presents the surface topography measurements performed on the different electrodes. Sec. V discusses additional vacuum considerations and measurements.

ACKNOWLEDGMENTS

The authors acknowledge the financial support by the Fédération Wallonie Bruxelles, through the project “iBEAM” and "REACSURF" funded by its research program “Actions de Recherche Concertées” (Convention No. 18/23-090 and No. 24/29-139, respectively) and by the Fonds de la Recherche Scientifique - FNRS. A.D. is a Research Director of the FNRS. X.U. is a Senior Research Associate of the Fonds de la Recherche Scientifique - FNRS. C.L. thanks the FNRS financial support (CDR grant No. J.0113.23 and MIS grant No. F.4038.24).

DATA AVAILABILITY STATEMENT

The data that support the findings of this study are available within the article.

AUTHOR DECLARATIONS

Conflict of Interest

The authors have no conflicts to disclose.

ACCEPTED MANUSCRIPT
Journal of Vacuum Science & Technology B
This is the author's peer reviewed, accepted manuscript. However, the online version of record will be different from this version once it has been copyedited and typeset.
PLEASE CITE THIS ARTICLE AS DOI: 10.1116/6.0005580

[1]H. S. Sonalikar and A. K. Mohanty, "Numerical study of segmented-electrode planar orbitraps," International Journal of Mass Spectrometry **417**, 58–68 (2017).
[2]L. A. Gill, J. W. Amy, W. E. Vaughn, and R. G. Cooks, "In situ optimization of the electrode geometry of the quadrupole ion trap," International journal of mass spectrometry **188**, 87–93 (1999).
[3]P. Szyszka, J. Jendryka, J. Sobków, M. Zychla, M. Białas, P. Knapkiewicz, J. Dziuban, and T. Grzebyk, "MEMS quadrupole mass spectrometer," Sensors and Actuators B: Chemical **411**, 135712 (2024).
[4]S. D. Gordon and A. Osterwalder, "3D-printed beam splitter for polar neutral molecules," Physical Review Applied **7**, 044022 (2017).
[5]M. Bergin, T. Myles, A. Radić, C. Hatchwell, S. Lambrick, D. Ward, S. Eder, A. Fahy, M. Barr, and P. Dastoor, "Complex optical elements for scanning helium microscopy through 3D printing," Journal of Physics D: Applied Physics **55**, 095305 (2022).
[6]N. Lazarus, "Metallization of 3D-printed devices," in *Resilient Hybrid Electronics for Extreme/Harsh Environments* (CRC Press, 2024) pp. 69–92.
[7]E. Redondo and M. Pumera, "Fully metallic copper 3D-printed electrodes via sintering for electrocatalytic biosensing," Applied Materials Today **25**, 101253 (2021).
[8]E. Vaněčková, M. Bouša, R. Sokolová, P. Moreno-García, P. Broekmann, V. Shestivska, J. Rathouskỳ, M. Gál, T. Sebechlebská, and V. Kolivoška, "Copper electroplating of 3D printed composite electrodes," Journal of Electroanalytical Chemistry **858**, 113763 (2020).
[9]A. Ambrosi and M. Pumera, "3D-printing technologies for electrochemical applications," Chemical society reviews **45**, 2740–2755 (2016).
[10]P. Wiebe, P. Beierle, H.-C. Shao, B. Gergely, A. F. Starace, and H. Batelaan, "Performance of plastic electron optics components fabricated using a 3D printer," Ultramicroscopy **205**, 70–74 (2019).
[11]K. Iyer, B. M. Marsh, G. O. Capek, R. L. Schrader, S. Tichy, and R. G. Cooks, "Ion manipulation in open air using 3D-printed electrodes," Journal of the American Society for Mass Spectrometry **30**, 2584–2593 (2019).
[12]P. Johnson, P. Copeland, A. Ayodele, E. Tarekegn, S. Bromley, W. Harrell, C. Sosolik, and J. Marler, "In-vacuum performance of a 3D-printed ion deflector," Vacuum **172**, 109061 (2020).
[13]C. Drees, S. Höving, W. Vautz, J. Franzke, and S. Brandt, "3D-printing of a complete modular ion mobility spectrometer," Materials Today **44**, 58–68 (2021).
[14]A. Schiller, S. Hoeving, M. Akermann, D. Schwendemann, J. Franzke, and S. Brandt, "Revolutionizing ion mobility spectrometry: Rapid and cost-efficient manufacturing of drift tubes using additive manufacturing with coaxial filament," Materials Today **83**, 113–124 (2025).
[15]K. K. Augusto, R. D. Crapnell, E. Bernalte, S. Zighed, A. Ehamparanathan, J. L. Pimlott, H. G. Andrews, M. J. Whittingham, S. J. Rowley-Neale, O. Fatibello-Filho, *et al.*, "Optimised graphite/carbon black loading of recycled PLA for the production of low-cost conductive filament and its application to the detection of β-estradiol in environmental samples," Microchimica Acta **191**, 375 (2024).
[16]M. J. Kim, M. A. Cruz, S. Ye, A. L. Gray, G. L. Smith, N. Lazarus, C. J. Walker, H. H. Sigmarsson, and B. J. Wiley, "One-step electrodeposition of copper on conductive 3D printed objects," Additive Manufacturing **27**, 318–326 (2019).
[17]A. Diaz, *Monolithically 3-D Printed, Quadrupole Mass Filter for High-Precision, Compact, CubeSat Mass Spectrometry*, Ph.D. thesis, Massachusetts Institute of Technology (2023).
[18]H. Guillén-Alonso, I. Rosas-Román, and R. Winkler, "The emerging role of 3d-printing in ion mobility spectrometry and mass spectrometry," Analytical Methods **13**, 852–861 (2021).
[19]L. Elviri, R. Foresti, A. Bianchera, M. Silvestri, and R. Bettini, "3D-printed polylactic acid supports for enhanced ionization efficiency in desorption electrospray mass spectrometry analysis of liquid and gel samples," Talanta **155**, 321–328 (2016).
[20]J. Fialova, J. Hrabak, V. Studentova, D. Kavan, P. Pompach, and P. Novak, "Three-dimensional printed target plates for matrix-assisted laser desorption/ionization mass spectrometry," Analytical chemistry **92**, 12783–12788 (2020).
[21]B. Tomasetti, C. Lauzin, and A. Delcorte, "Enhancing ion signals and improving matrix selection in time-of-flight secondary ion mass spectrometry with microvolume expansion using large argon clusters," Analytical Chemistry **95**, 13620–13628 (2023).
[22]B. Tomasetti, J. Fréreux, X. Urbain, T. Schiltz, A. Lorvelec, C. Dupont-Gillain, A. Delcorte, and C. Lauzin, "Cluster assisted soft-landing hub (CLASH): An instrument for surface desorption and deposition using a pulsed cluster ion source," Review of Scientific Instruments (2026), accepted for publication.
[23]P. Sosnowski and G. Hopfgartner, "Application of 3D printed tools for customized open port probe-electrospray mass spectrometry," Talanta **215**, 120894 (2020).
[24]L. H. Tucker, A. Conde-González, D. Cobice, G. R. Hamm, R. J. Goodwin, C. J. Campbell, D. J. Clarke, and C. L. Mackay, "Maldi matrix application utilizing a modified 3D printer for accessible high resolution mass spectrometry imaging," Analytical chemistry **90**, 8742–8749 (2018).
[25]C. Ricketts, B. Cooper, G. Edwards, H. Perrett, J. Billowes, C. Binnersley, T. Cocolios, K. Flanagan, R. G. Ruiz, R. de Groote, *et al.*, "A compact linear paul trap cooler buncher for CRIS," Nuclear Instruments and Methods in Physics Research Section B: Beam Interactions with Materials and Atoms **463**, 375–377 (2020).
[26]S. Xu, X. Xia, Q. Yu, A. Parakh, S. Khan, E. Megidish, B. You, B. Hemmerling, A. Jayich, K. Beck, *et al.*, "3D-printed micro ion trap technology for quantum information applications," Nature **645**, 362–368 (2025).
[27]C. A. Deckert, "Electroless copper plating," in *Surface Engineering* (ASM International, 1994) pp. 311–322.
[28]J. G. Wright, B. P. Charnay, J. A. Rabinowitz, R. G. Mariano, and M. W. Kanan, "Rapid prototyping of lab-scale electrolysis cells using stereolithography and electroless plating," Device **1** (2023).
[29]K. Drallios, G. Pham, A. Cuccaro, M. Karthikeyan, T. Loke, J. Tence, and T. M. O. Popp, "Metallized, 3D-printed radiofrequency coils," Journal of Magnetic Resonance , 108057 (2026).
[30]Polymertal, "Polymertal – the best of both worlds: Polymers and metals," `https://polymertal.com/` (2026), accessed: 2026-04-01.
[31]M. Proyavin, A. Vikharev, A. Fedotov, D. Sobolev, N. Y. Peskov, P. Makhalov, M. Y. Shmelev, and S. Kuzikov, "Development of electrodynamic components for microwave electronic devices using the technology of 3D photopolymer printing with chemical surface metallization," Radiophysics and Quantum Electronics **63**, 469–478 (2020).
[32]M. D. Proyavin, M. V. Morozkin, N. S. Ginzburg, A. N. Denisenko, M. V. Kamenskiy, V. E. Kotomina, V. N. Manuilov, A. A. Orlovskiy, I. V. Osharin, N. Y. Peskov, *et al.*, "Experimental studies of microwave tubes with components of electron–optical and electrodynamic systems implemented using novel 3D additive technology," Instruments **6**, 81 (2022).
[33]R. Bejjani, A. Roucou, X. Urbain, K. Moshkunov, G. Vanlancker, and C. Lauzin, "STARGATE: A new instrument for high-resolution photodissociation spectroscopy of cold ionic species," Review of Scientific Instruments **92** (2021).
[34]R. Bejjani, *Conception, construction and validation of scientific instruments to study the spectrum of cold ionic species*, Ph.D. thesis, Université Rennes 1; Université catholique de Louvain (1970-....) (2021).
[35]B. Tomasetti, M. Lakhdar, V. Delmez, C. Dupont-Gillain, C. Lauzin, and A. Delcorte, "Gas cluster ion beam-assisted deposition for fabricating dry multilayers containing enzyme and substrate with on-demand release," ACS Applied Materials & Interfaces **16**, 37248–37254 (2024).
[36]H. E. D. Prints, "Electroplating 3d prints | new graphite tutorial," (2024), accessed: 2025-03-24.